Bioelectrochemistry 134 (2020) 107528

Contents lists available at ScienceDirect

Bioelectrochemistry

journal homepage: www.elsevier.com/locate/bioelechem

In vitro attenuation of astrocyte activation and neuroinflammation through ibuprofen-doping of poly(3,4-ethylenedioxypyrrole) formulations

Katarzyna Krukiewicz [a,b,*], Agnieszka Kowalik [b], Roman Turczyn [b], Manus J.P. Biggs [a]

[a] Centre for Research in Medical Devices, National University of Ireland, Galway, Newcastle Road, H91 W2TY Galway, Ireland
[b] Department of Physical Chemistry and Technology of Polymers, Silesian University of Technology, M.Strzody 9, 44-100 Gliwice, Poland

ARTICLE INFO

Article history:
Received 15 December 2019
Received in revised form 31 March 2020
Accepted 2 April 2020
Available online 8 April 2020

Keywords:
Conducting polymers
Drug delivery
Ibuprofen
Neuroinflammation
Neural interfaces
Poly(3,4-ethylenedioxypyrrole)

ABSTRACT

Neuroinflammation is often associated with poor functional recovery and may contribute to or initiate the development of severe neurological disorders, such as epilepsy, Parkinson's disease or Alzheimer's disease. Ibuprofen (IBU), being one of the most commonly used non-steroidal anti-inflammatory drugs, is known to possess neuroprotective activity and serve as a promising therapeutic for the treatment of neuroinflammation. In this study, the potential of an IBU-loaded poly(3,4-ethylenedioxypyrrole) (PEDOP) matrix has been assessed as a neural interface material with an aim to control astrocyte activation and suppress neuroinflammation in vitro. Three types of drug immobilization protocols were investigated, leading to the fabrication of IBU-loaded PEDOP matrices exhibiting a broad spectrum of electrical characteristics, drug release profiles, as well as biological responses. Among all investigated PEDOP formulations, PEDOP matrices formed through a three-step immobilization protocol exhibited the highest charge storage capacity (30 ± 1 mC/cm^2) as well as a double layer capacitance of 645.0 ± 51.1 μF, associated with a relatively enlarged surface area. Demonstrating a total drug loading capacity of 150 μg/ml and a release rate constant of 0.15 1/h, this coating formulation may be employed as a safe electrical conducting drug eluting system.

1. Introduction

Neuroinflammation, defined as an inflammatory response within the central or peripheral nervous system, can be associated with mechanical trauma, infection or neurodegenerative disease [1,2]. The neuroinflammatory response can be described as a composition of overlapping cytotoxic and cytotrophic processes, which in evolved organisms are regulated in order to promote homeogenesis of the nervous system [3]. Regardless of the source of neuroinflammation, this state is often associated with delayed recovery [1], and chronic brain inflammation is a key barrier to regeneration [3]. Critically, prolonged inflammation may contribute to the formation of disease pathogenesis across the central nervous systems and the development of neurological disorders [2]. For instance, disregulation of inflammatory cell activation in the neural tissue injuries is seen to be associated with the development of epilepsy in humans [4]. Recently, inflammation has also acquired relevance as one of the principal mechanisms of neuronal dysfunction in Parkinson's disease [5], β-amyloid pathology and the progression of Alzheimer's disease [6].

Although non-steroidal anti-inflammatory drugs (NSAIDs) are known to exhibit neuroprotective functions, the origins of these effects are not yet well-known [7,8]. One of the most commonly used over-the-counter NSAIDs is *iso*-butylphenylpropionic acid, also known as ibuprofen (IBU). IBU is a potent free radical scavenger that can reduce free radical generation, and is known to decrease the production of nitric oxide, protect neurons against glutamate toxicity and decrease the production of proinflammatory cytokines in humans [9,10]. IBU has been also shown to down-regulate the inflammatory response induced by traumatic brain injury [11], protect dopaminergic cells and slow down the progression of Parkinson's disease [12], as well as exhibit neuroprotective effects against Alzheimer's [9] and Machado-Joseph diseases [13] in vivo. Because of its neuroprotective activity, relative safety, and long history of use, IBU may serve as a promising therapeutic for the treatment of neuroinflammation [9]. To maximize the efficacy of NSAIDs in central nervous tissue and avoid off site-effects, various strategies for localized drug delivery have been

* Corresponding author at: Centre for Research in Medical Devices, National University of Ireland, Galway, Newcastle Road, H91 W2TY Galway, Ireland.
E-mail address: katarzyna.krukiewicz@polsl.pl (K. Krukiewicz).

https://doi.org/10.1016/j.bioelechem.2020.107528
1567-5394/

investigated in vivo [14]. Of particular interest in neurospecific applications are drug-loaded conducting polymers matrices which may serve as precisely controlled drug delivery platforms [1516] that can be controlled through an electrical signal [17]. Indeed, conducting polymer systems have already been successfully applied for the controlled release of NSAIDs, particularly naproxen [16] and ibuprofen [18,19].

In this paper, the electrochemical performance, drug release profile and neuronal response to IBU-loaded poly(3,4-ethylenedioxypyrrole) (PEDOP) matrices is assessed. Although the most frequently used conducting drug carriers are poly(3,4-et hylenedioxythiophene) (PEDOT) and polypyrrole (PPy), their structural analogue, PEDOP, exhibits a combination of the advantages of its "parent" polymers and is devoid of some of their disadvantages. In contrast to EDOT, EDOP is soluble in water and can be electropolymerized under aqueous conditions [20]. Similarly to PEDOT [21], due to the presence of dioxyethylene bridging group, PEDOP is supposed to exhibit higher electrochemical stability than PPy. Furthermore, PEDOP has been described previously as exhibiting neurocytocompatibility [22], and having a general potency to serve as a drug carrier in vitro [18]. The low oxidation potential of EDOP enables to initialize the process of polymerization at lower potential than for EDOT [20], making PEDOP an efficient drug carrier also for biologically active compounds which are prone to oxidative degradation. Herein, three different types of IBU immobilization protocols, drug release profiles, as well as biological response of IBU-loaded PEDOP matrices were investigated and characterized in vitro. Finally, the optimized conditions for the fabrication of an electroactive conducting polymer coating with superior electrochemical characteristics and enhanced neuroprotective functionality in vitro is presented.

2. Materials and methods

2.1. Drug immobilization

The process of electrochemical polymerization was performed by means of a PARSTAT 2273 potentiostat in a three-electrode set-up, comprising a Pt-coated Thermanox coverslip (Electron Microscopy Sciences) as a working electrode, Ag/AgCl (3 M KCl) (EDAQ) as a reference electrode and a glassy carbon rod as an auxiliary electrode. 10 mM 3,4-ethylenedioxypyrrole (EDOP, 2% (w/v) in THF, Sigma Aldrich) was polymerized in a course of a cyclic voltammetry (CV) in the aqueous solutions of either 0.1 M sodium *p*-toluenesulfonate (PTS, 95%, Sigma Aldrich) to form P-PTS matrix, or 0.1 M ibuprofen sodium salt (IBU, ≥98%, Sigma-Aldrich) to form P-IBU(1) matrix, or 0.1 M PTS and 0.1 M IBU to form P-IBU(2) matrix. In each case, the geometrical surface area of the working electrode was equal to 0.283 cm^2. CV curves were collected at the scan rate of 0.1 V/s for 50 CV cycles within the potential range between −0.5 V and 0.9 V (vs. Ag/AgCl). P-IBU(3) matrix was formed in the course of a three-step immobilization protocol [23], comprising a) the electrochemical polymerization of EDOP (10 mM) in 0.1 M PTS aqueous solution, followed by b) dedoping of P-PTS matrix through chronoamperometric reduction at −0.5 V (vs. Ag/AgCl) in 0.1 M PTS aqueous solution for 600 s and c) secondary doping in the presence of 0.1 M IBU aqueous solution by chronoamperometric oxidation at 0.5 V (vs. Ag/AgCl) for 600 s. The potentials of chronoamperometric reduction and oxidation were selected basing on the CV curves of PEDOP to allow the matrix to be fully reduced/oxidized. Grade 1 (R > 10 MΩ/cm) deionised water was employed as a solvent for preparation of all used solutions.

2.2. Material characterization

A PARSTAT 2273 potentiostat was used for the electrochemical studies performed in a three-electrode set-up as described above. CV curves were collected in a physiologically relevant phosphate buffered saline solution (PBS, 0.01 M Na_2HPO_4, 0.0018 KH_2PO_4, 0.0027 M KCl and 0.137 M NaCl, pH = 7.4, Sigma Aldrich), within the potential range from −0.7 to 0.7 V (vs. Ag/AgCl) at 0.1 V/s for 5 CV cycles. CV curves were used to determine charge storage capacity (CSC), calculated as the electric charge integrated under a corresponding CV curve during one CV cycle [19], according to the formula:

$$CSC = \int_{t_1}^{t_2} I(t)dt \quad (1)$$

where t_1 is the time of beginning of a CV cycle (s), t_2 is the time of end of a CV cycle (s), and I is the current density (A/cm^2).

EIS spectra were collected in a PBS solution within a frequency range from 100 mHz to 100 kHz, with an AC amplitude of 40 mV (vs. Ag/AgCl) and a DC potential of 0 V (vs. Ag/AgCl). The results were presented on Bode plots and compared to those of a bare Pt electrode. EIS Spectrum Analyzer 1.0 software [24] and the Powell algorithm were used to fit the experimental data to an equivalent circuit model. Capacitance was calculated basing on the parameters of a constant phase element (CPE) according to the formula:

$$C = \frac{(P \cdot R)^{1/n}}{R} \quad (2)$$

where C is the capacitance (F), R is the film resistance (Ω), P and n are CPE parameters.

The chemical structure of polymer matrices was characterized by means of a Raman spectroscopy using Renishaw InVia confocal microRaman system equipped with a laser operating at 830 nm and a CCD detector. Raman spectra were acquired in the spectral range between 300 and 1800 cm^{-1}. The surface morphology of polymer matrices was studied by means of a Hitachi S-4700 Scanning Electron Microscope operating at 15 kV. ImageJ (NIH) image analysis software was used to quantify the sizes of polymer grains. Origin software was used to plot histograms with normal distribution curve overlays. Thickness of samples was determined by means of a Profilm3D Profilometer and 3D Optical Profiler (Filmetrics). The results were expressed as a mean of at least 12 measurements ± standard deviation.

2.3. Drug release studies

The release experiments were conducted according to the previously developed protocol [25]. Briefly, Pt-coated Thermanox coverslips coated with P-IBU(1), P-IBU(2) and P-IBU(3) were immersed in 1 mL PBS solution and left under gentle shaking (80 rpm, 37 °C) for 14 days. 0.2 mL of the supernatant was taken at specific time points (1 h, 3 h, 6 h, 8 h, 24 h, 2 days, 4 days, 6 days, 8 days, 10 days, 12 days and 14 days) which was supplemented with 0.2 mL of a fresh PBS solution to keep a constant elution volume of 1 mL. This procedure allowed the maintenance of a so-called sink condition preventing the saturation of the supernatant with IBU. The concentration of released IBU was determined through UV–Vis spectrophotometry with the use of a Thermo Scientific Evolution 60S Spectrophotometer (Thermo Fisher Scientific, Waltham, MA, USA) and was based on the absorbance at the peak characteristic for IBU (264 nm) (Fig.S1A). IBU concentration in solution was determined through a calibration curve (Fig.S1B) plotted for absorbance versus drug concentration. A linear relationship was observed between 0.001 mM and 1.0 mM IBU satisfying the equation y = 0 .4x + 0.01 (R^2 = 0.999). The measurements were performed for four

technical replicas and the results were expressed as a mean ± standard deviation.

Two models were used to analyze the release kinetics:

(a) power equation [26]:

$$\frac{M_t}{M_\infty} = Kt^n \tag{3}$$

rearranged to its linear form:

$$\log\left(\frac{M_t}{M_\infty}\right) = \log k + n\log t \tag{4}$$

where: M_t is the amount of drug released at time t, M_∞ is the amount of drug at the equilibrium state, k is the release rate constant, and n is the exponent of release related to drug release mechanism.

(b) Avrami's equation [27].

$$X = 1 - \exp(-kt^n) \tag{5}$$

rearranged to its linear form:

$$\ln(-\ln(1-X)) = \ln k + n\ln t \tag{6}$$

where: X is the fraction of a drug released at time t, n is the Avrami parameter and k is the release rate constant.

The fitting of the data describing the release kinetics was made with the use of two free parameters, namely n and k. The equilibrium concentration was determined experimentally.

2.4. Biological characterization

The cytocompatibility of P-PTS, P-IBU(1), P-IBU(2) and P-IBU(3) formulations was determined with respect to a primary mixed neural population obtained from the mesencephalon of embryonic Sprague-Dawley rats, and cultured for 3, 7 and 14 days, according to a previously developed protocol [28]. The cellular composition on control and PEDOP-coated Pt electrodes was assessed by immunofluorescence markers for astrocytes (GFAP) and neurons (β-tubulin III), and the fluorescent images were collected by an Olympus Fluoview 1000 Confocal Microscope (Olympus, Tokyo, Japan). Cell density and the average number of astrocytes were analyzed by counting the number of nuclei corresponding to neurons and astrocytes in an area of 900 μm^2 in at least 20 random images taken from test and control groups [29]. The same sets of fluorescent images were used to determine the mean area of astrocytes, as carried out with the use of ImageJ (NIH) image analysis software.

The biological experiments were conducted to include three biological replicas for all test and control groups. The results were expressed as a mean ± standard deviation or standard error of the mean. One-way Anova and t-test were performed to determine the statistical significance ($p < 0.05$).

3. Results and discussion

3.1. Electrochemical characterization

The immobilization of a drug into a conducting polymer matrix during synthesis is typically employed in order to balance positive charges caused by the oxidation of the growing polymer chain. Therefore, if the drug has an anionic structure, it can act as a primary doping ion. Some strategies, however, involve the use of a mixed electrolyte, namely a primary dopant and a drug co-dopant, to facilitate the process of electropolymerization. Alternatively, drug molecules can be incorporated into conducting matrix following polymer synthesis, and this process is based on an ion-exchange mechanism between the primary dopant, which is removed from the matrix during electrochemical reduction, and drug molecules, which are incorporated in the polymer matrix during electrochemical oxidation. These three immobilization strategies result in the formation of polymer matrices possessing different characteristics in terms of electrochemical properties, drug loading capacity and drug release kinetics. Here, drug-loaded PEDOP matrices were formulated via three immobilization protocols as summarized in Scheme 1, leading to the formation of three IBU-loaded PEDOP-based systems, namely P-IBU(1), P-IBU(2) and P-IBU(3).

The corresponding cyclic voltammetric (CV) curves of electrochemical polymerization, presented in Fig.S2A–C, indicate that in all cases the monomer was irreversibly oxidized and a conductive film was electrodeposited onto a Pt electrode. The thickness of as-formed polymer films was comparable, achieving the highest value for P-PTS (332 ± 61 nm) and slightly lower values for IBU-loaded PEDOP: 307 ± 58 nm, 282 ± 47 nm and 304 ± 64 nm, for P-IBU (1), P-IBU(2) and P-IBU(3), respectively. The CV curves recorded during the polymerization of EDOP in the presence of IBU exhibited oxidation peaks at a potential of 0.5/0.6 V (vs. Ag/AgCl). The obtained chronoamperometric curves (Fig.S2D) were typical for a three-step immobilization procedure.

After the synthesis, all PEDOP-based matrices were further examined to assess their electrochemical properties. CV curves were obtained from electrodeposited PEDOP and IBU-loaded PEDOP matrices, namely P-PTS, P-IBU(1), P-IBU(2) and P-IBU(3), as well as from bare Pt electrodes (Fig. 1A). It was observed that the area under the CV curves (equivalent to charge passing through the modified electrode) obtained from P-PTS and P-IBU(3) coated Pt electrodes was more developed than the area under CV curves obtained from P-IBU(1) and P-IBU(2) coatings. The beneficial effect of a three-step immobilization procedure on the electrochemical properties of the resulting material was revealed when assessing the charge storage capacity (CSC) [30] of all investigated PEDOP formulations (Fig. 1B). Here, the P-IBU(3) coating was observed to exhibit a CSC value of 30 ± 1 mC/cm^2, significantly higher than was in the case of P-IBU(1) (22 ± 2 mC/cm^2), P-IBU(2) (21 ± 1 mC/cm^2), as well as a bare Pt electrodes (7 ± 1 mC/cm^2), indicating that P-IBU(3) fims were able to store the highest charge before reaching overpotential and undergoing irreversible faradaic reactions relative to other investigated matrices.

Similarly, the behaviour of an electric charge passing through the electrode and the electrode coating was determined by means of electrochemical impedance spectroscopic (EIS) studies as shown in Fig. 2A (impedance modulus vs. frequency) and Fig. 2B (phase angle vs. frequency). Analysis of the Bode impedance and phase plots for pristine PEDOP and IBU-loaded PEDOP matrices indicated that P-PTS and P-IBU(3) demonstrated similar mechanism of charge transfer. Likewise P-IBU(1) and P-IBU(2), which also demonstrated similar mechanism of charge transfer. It can be inferred that this effect is due to the presence of a co-dopant, IBU, within the whole volume of PEDOP matrix, which is not the case when IBU is immobilized after the process of electrochemical polymerization (as with a P-IBU(3) matrix).

A detailed investigation of the charge transfer was possible through the simulation of EIS data with an equivalent circuit model. Basing on the visual investigations of collected spectra, particularly Bode phase plots, two equivalent circuits were proposed for the description of charge transfer occuring within investigated samples. Since in the case of P-IBU(3) drug molecules are expected to be immobilized at the near surface region of the polymer matrix rather than in bulk, the mechanism of charge transfer for P-IBU(3) is supposed to resemble more the mechanism of charge transfer for P-PTS than for P-IBU(1) and P-IBU(2). Consequently, for P-PTS and

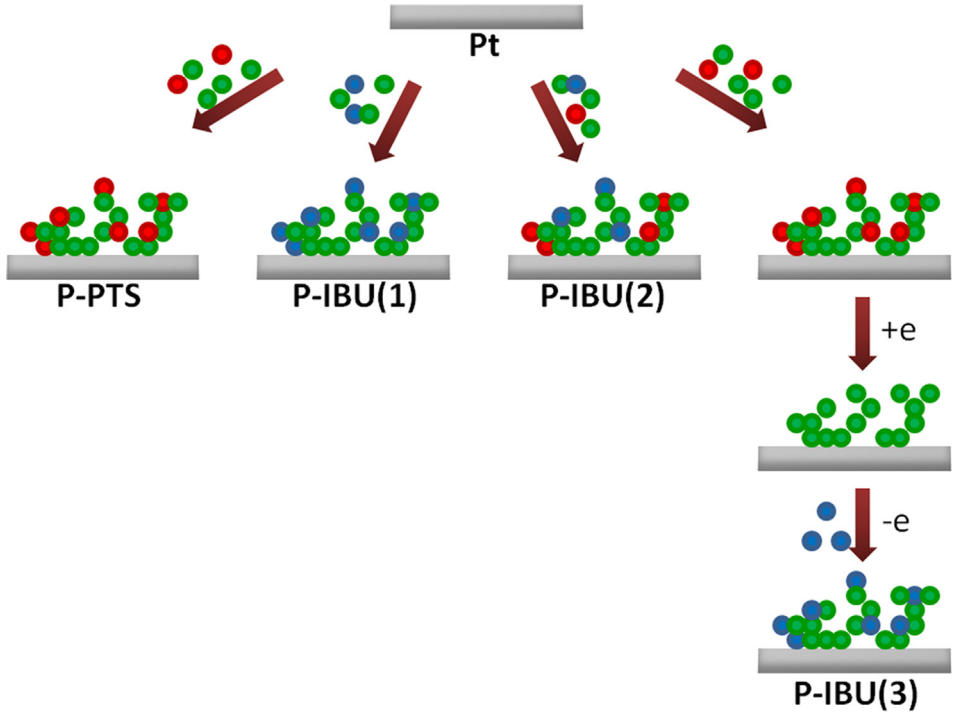

Scheme 1. Schematic representation of the fabrication routes leading to the formation of P-PTS, P-IBU(1), P-IBU(2) and P-IBU(3) on the surface of Pt-coated electrodes; green dots represent EDOP, red dots represent PTS, and blue dots represent IBU.

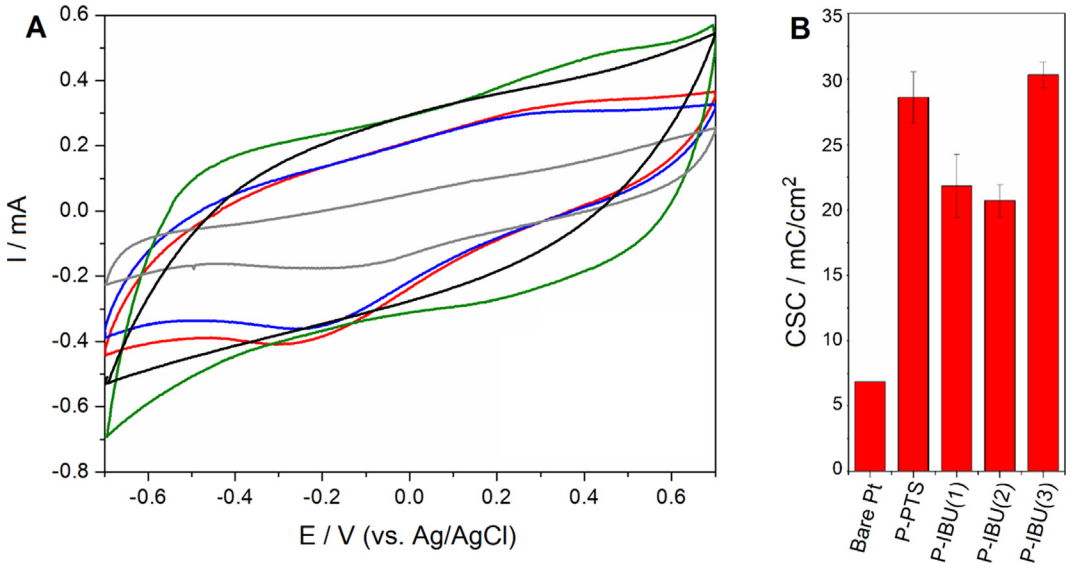

Fig. 1. CV curves (A) and corresponding charge storage capacities, CSC (B) of PEDOP and IBU-loaded PEDOP matrices, P-PTS (black line), P-IBU(1) (red line), P-IBU(2) (blue line) and P-IBU(3) (green line), as well as a bare Pt electrode (gray line).

P-IBU(3), a modified Randles circuit was employed (Fig. 2C), comprising a parallel combination of a solution resistance (R_S), charge transfer resistance (R_{CT}), double layer capacitance (C_{DL}) and constant phase element (CPE_P) associated with the capacitance (C_P) of the polymer matrix. The model resulted in the good fit between the experimental and simulated data (2.7% and 2.2% deviation for P-PTS and P-IBU(3), respectively). To properly model P-IBU(1) and P-IBU(2), it was necessary to add one more circuit element (red square in Fig. 2C) responsible for the diffusion of drug molecules (W_D) and associated resistance (R_D), forming the equivalent circuit model similar to the one developed prevously for PEDOP [20]. The additional capacitive element, giving rise to a capacitive peak at approx. 100 Hz in the phase plot of P-IBU(1) and P-IBU (2) (Fig. 2B), should be related to the diffusion of drug molecules within polymer matrix as the result of spontaneous release of IBU occuring during the measurement. Also here, the model resulted in a good fit between the experimental and simulated data (0.9% and 1.9% deviation for P-IBU(1) and P-IBU(2), respectively). The EIS fitting parameters for PEDOP and IBU-loaded PEDOP matrices are summarized in Table S1.

Since the charge transfer resistance of a bare Pt electrode was calculated to equal 17.2 ± 1.5 kΩ, all PEDOP formulations are

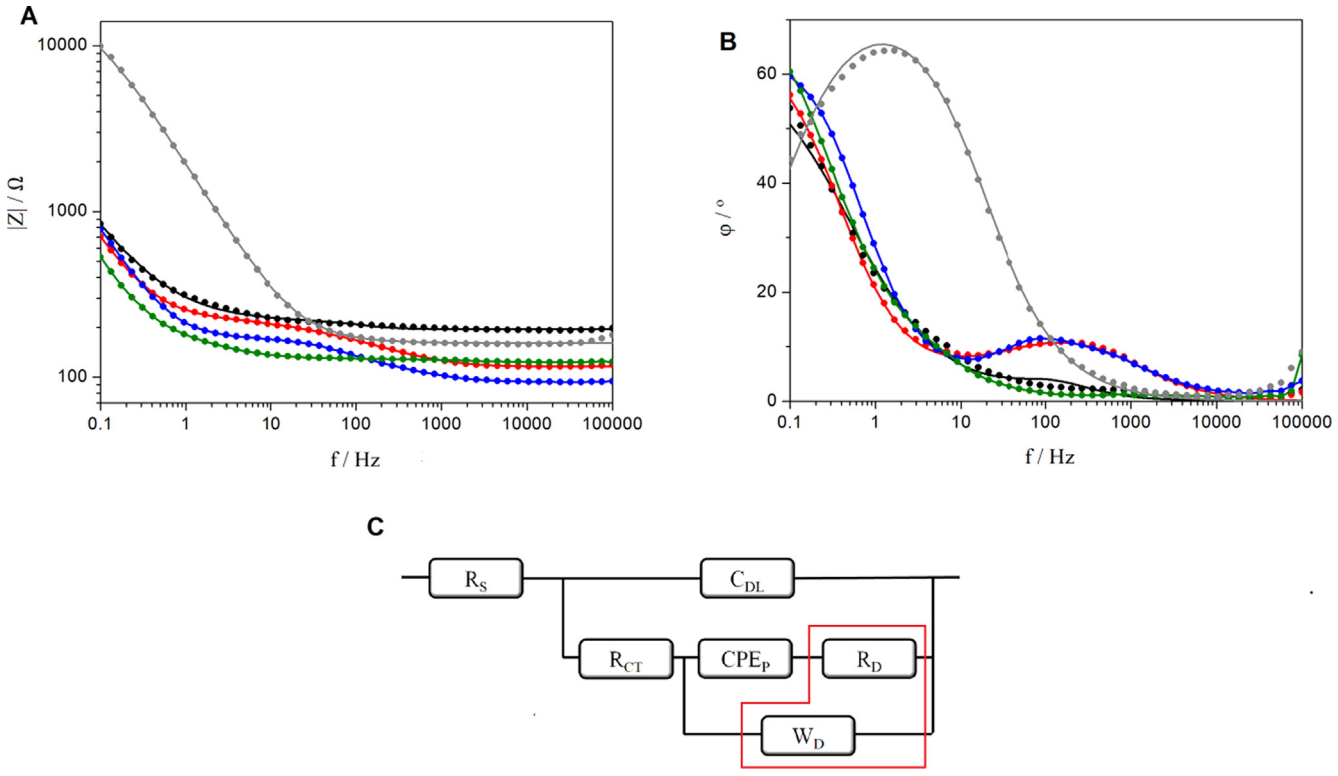

Fig. 2. EIS results in the form of Bode plots of impedance modulus vs. frequency (A) and phase angle vs. frequency (B) for PEDOP and IBU-loaded PEDOP matrices, namely P-PTS (black), P-IBU(1) (red), P-IBU(2) (blue) and P-IBU(3) (green), as well as a bare Pt electrode (gray); dots represent experimental data, while lines represent simulated results. Equivalent circuit model used for the fitting of EIS data (C), red square indicates the components associated with the diffusion of drug molecules occuring in P-IBU(1) and P-IBU(2).

shown to significantly contribute to a decrease in the overall impedance moduli of the electrode. The charge transfer resistance varied between 43 ± 5 Ω for P-IBU(3) matrices and 10 ± 1 Ω for P-IBU(1) matrices, but it should be noted that although all polymer formulations exhibited low R_{CT} valuses, additional resistive factor associated with the diffusion of IBU should be considered. The depletion of the IBU dopant through spontaneous release leads to diffusional limitations increasing matrix resistance. The P-IBU(3) matrix was also found to exhibut the highest double layer capacitance (645.0 ± 51.1 μF), which could be correlated to its developed surface area (see Section 3.2).

3.2. Material characterization

The chemical structure of all experimental PEDOP chemistries was confirmed through Raman analysis (Fig. 3). which indicated characteristic PEDOP peaks attributable to the asymmetric stretching mode of C=C bonds of pyrrole (1613 cm^{-1}), the symmetric stretching mode of C=C—O groups of PEDOP (1396 cm^{-1}), the C—C stretching mode (low intensity peaks in the range of 1300–1350 cm^{-1}), the C—N stretching of the pyrrole rings (1186 cm^{-1}), the N—H vibrations (1020 cm^{-1}) and the N—H out-of-plane bending mode (706 cm^{-1}) [18,31,32]. The presence of PTS dopant in P-PTS polymer formulations was confirmed by the appearance of a peak assigned to symmetric SO_3^- bending at 634 cm^{-1} [33]. The disappearance of this signal in the Raman spectrum of P-IBU(3) proves that the conditions of dedoping were sufficient to entirely remove PTS from the near surface region of the polymer matrix. The presence of IBU moiety in all IBU-loaded matrices: P-IBU(1), P-IBU(2) and P-IBU(3), was confirmed by the appearance of bands characteristed for the IBU molecule (Fig.S3), namely the out of plane C—C ring deformation (484 cm^{-1}), in plane C—H ring bending

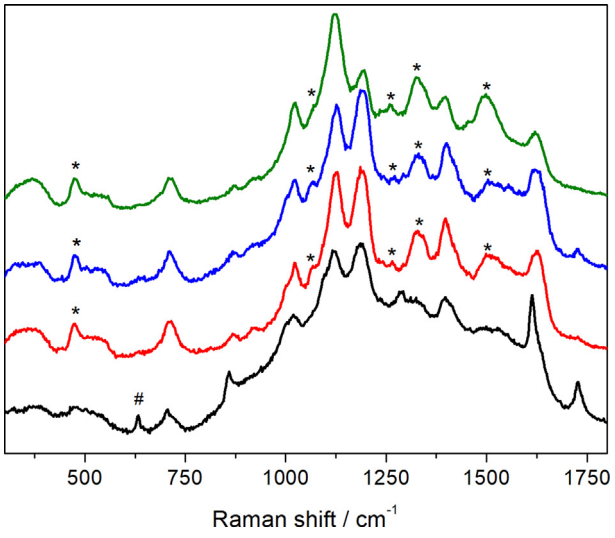

Fig. 3. Raman spectra of PEDOP and IBU-loaded PEDOP matrices, namely P-PTS (black), P-IBU(1) (red), P-IBU(2) (blue) and P-IBU(3) (green); * and # are used to mark the bands characteristic for IBU and PTS, respectively.

(1062 and 1342 cm^{-1}), C—C ring stretching (1264 cm^{-1}), as well as C—H deformations (1502 cm^{-1}) [34]. Therefore, all three drug immobilization protocols were shown to be efficient for entrapment of IBU moieties inside PEDOP matrix.

Chemical doping is known to have a strong effect on the morphology of conducting polymer formulations [20]. As shown in Fig. 4A, the surface of electrodeposited P-PTS films was composed of polymer grains with an average diameter of ~0.6 μm, and which

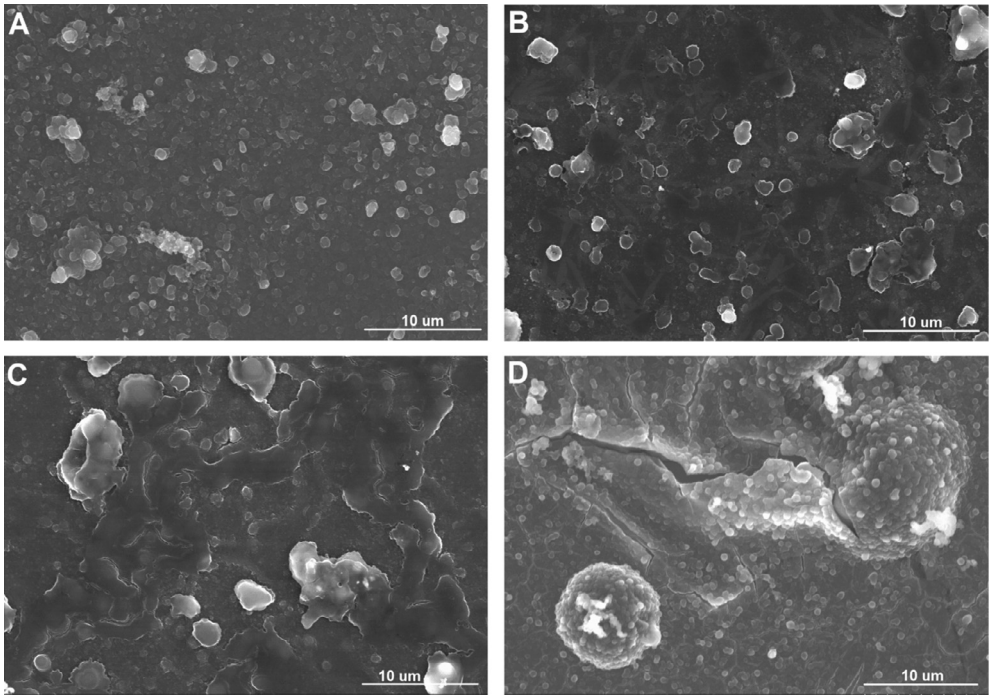

Fig. 4. Representative scanning electron microscope images of PEDOP and IBU-loaded PEDOP matrices, namely P-PTS (A), P-IBU(1) (B), P-IBU(2) (C) and P-IBU(3) (D).

were regularly dispersed over the Pt electrode. When IBU was incorporated as a primary dopant (P-IBU(1)), the polymer grains were grouped into agglomerates with an average diameter of 1.4 μm (Fig. 4B). Conversely, the concurrent presence of both doping ions, namely PTS and IBU, enhanced the formation of a compact surface layer, in which the polymer grains were no longer individual structures (Fig. 4C). The electrochemical reduction and re-oxidation of the initial P-PTS matrix, through a three-step procedure of IBU immobilization, led to noticeable surface erosion and matrix stress during the ion exchange process. Interestingly, the initial globular structure (particles with an average diameter of 0.5 μm) was maintained in P-IBU(3) films (Fig. 4D) which could partially contribute to the enhanced electrochemical performance of this matrix as previously observed in PEDOT formulations [35]. Similar morphological reversibility during doping and dedoping processes has been already observed by Schoetz et al. [36], who investigated charging and discharging of PEDOT by atomic force microscopy. Noteworthly, the distribution of average diameters of polymer grains of P-IBU(3) films (Fig.S4D) resembled the standard normal size distribution, in contrast to other PEDOP formulations (Fig.S4A–C). Due to the presence of polymer grain agglomerates, P-IBU(2) was found to diverge significantly from a normal size distribution.

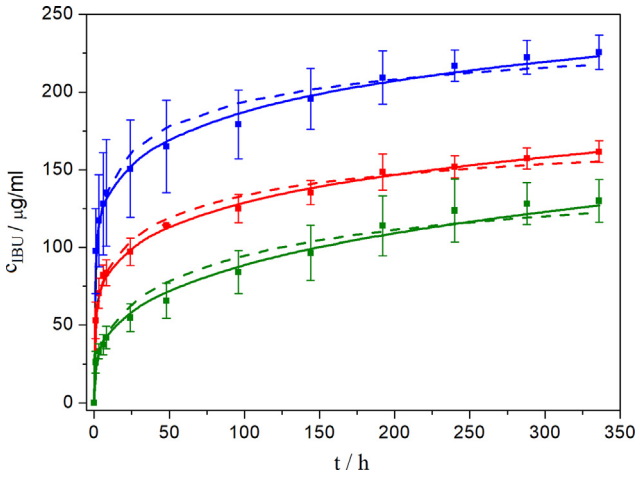

Fig. 5. Drug elution profiles of spontaneous IBU release from IBU-loaded PEDOP matrices, namely P-IBU(1) (red), P-IBU(2) (blue) and P-IBU(3) (green); dots are the experimental values, and lines represent the corresponding fitted curves calculated by means of power equation (solid lines) and Avrami's equation (dash lines).

3.3. In vitro IBU release studies

The suitability of PEDOP formulations for drug delivery was verified by IBU elution studies under spontaneous release conditions over a period of 14 days. The drug release profiles of IBU-loaded PEDOP matrices, namely P-IBU(1), P-IBU(2) and P-IBU(3) are presented in Fig. 5, indicating both the experimental values as well as the corresponding fitted curves calculated by means of power and Avrami's models. Power equation is a well-established semi-empirical model frequently used to describe drug release from polymeric systems [37,38]. Although Avrami's equation was originally used to describe crystallization mechanisms, it has been also used many times for the description of release kinetics [39–41], especially for conducting polymer based drug delivery systems [27,42–45]. In our case, the use of power law resulted in higher values of the correlation coefficient (R^2 = 0.99 for all three IBU-loaded PEDOP matrices) than the use of Avrami's model (R^2 between 0.96 and 0.98) (Table 1). Also the visual investigation of the fitted curves (solid and dash lines in Fig. 5 representing fitted curves calculated by means of power or Avrami's equations, respectively), demonstrated that the power law is describing the kinetics of release in a better way than Avrami's model. Particularly, fitting for Avrami's model led to the overestimation of the concentration of released drug in the first 7 days of release, and the underestimation of IBU concentration in longer periods. Both models gave the values of the exponent of release (n) lower than 1. Since in both models n is related to the drug release mechanism, its value indicates that

Table 1
Release kinetic parameters calculated basing on power and Avrami's equations for the spontaneous release of IBU from IBU-loaded PEDOP matrices.: k – release rate constant, n – release exponent, $t_{0.95}$ – time necessary for the release of 95% of immobilized drug, R^2 – correlation coefficient.

	Power equation				Avrami's equation			
	k, 1/h	n	$t_{0.95}$, days	R^2	k, 1/h	n	$t_{0.95}$, days	R^2
P-IBU(1)	0.31	0.18	19	0.99	0.33	0.31	53	0.98
P-IBU(2)	0.39	0.14	22	0.99	0.45	0.26	60	0.96
P-IBU(3)	0.16	0.29	21	0.99	0.15	0.42	54	0.96

the release of IBU from IBU-loaded PEDOP matrices has a diffusive character [38,42]. This is consistent with previous literature reports on polypyrrole-based drug delivery systems, for which a diffusive mechanism was found at open circuit conditions (spontaneous release) [27,42,45]. According to Papadopoulou et al. [46], such low values of *n* may occur in highly disordered matrices, which differ much from the percolation cluster.

The highest IBU release rate constant (0.45 1/h and 0.39 1/h according to the Avrami's and power models, respectively) was noted in P-IBU(2) formulations, corresponding to approx. 225 μg/ml IBU released over a period of 14 days. Further simulation with power kinetic parameters indicated that 95% of the total amount of immobilized IBU (250 μg/ml) will be eluted within 22 days. The release of IBU from both P-IBU(1) and P-IBU(3) formulations was reduced relative to P-IBU(2) formulation which was supposed to arise from IBU acting as a main dopant, necessary for maintaining the electroneutrality of the polymer. Here, over a period of 14 days only 160 μg/ml and 130 μg/ml of IBU was eluted for P-IBU(1) and P-IBU(3), respectively, and the release of 95% of the total amount of immobilized IBU (200 μg/ml and 150 μg/ml, respectively) was accomplished in circa 20 days (according to power equation).

Although a high drug loading capacity would seem to be an indicator of an efficient drug carrier, achieving a gradual, constant release of the optimal portion of drug over a prolonged time should be considered the ultimate goal of an ideal drug release system. According to recent studies, high doses of IBU could be hazardous in specific applications. In particular, IBU is used to close the ductus arteriosus in cases of neonate hyperbilirubinemia. Berns et al. [47] investigated bilirubin-associated brain damage in premature infants, showing that IBU delivery above a concentration of 125 μg/ml could interfere with bilirubin–albumin binding, decreasing neuron viability. Therefore, even though exhibiting the lowest drug loading capacity in this study (150 μg/ml) and the slowest release rate constant (approx. 0.15 1/h), P-IBU(3) could be considered as the most beneficial and the safest drug eluting system among all investigated IBU-loaded PEDOP matrices for neural applications.

3.4. Biological characterization

In order to evaluate the cytocompatibility of IBU doped PEDOP formulations, the analysis of cell density of astrocyte and neuron populations, and astrocyte activation, observed as the increase in astrocyte cell area [48], was assessed in vitro. Consequently, the analysis of the density of astrocyte and neuron populations on bare Pt and PEDOP-coated Pt electrodes (Fig. 6) revealed a significant decrease in the presence of astrocytes and an increase in the presence of neurons for all PEDOP-coated Pt electrodes with respect to bare Pt substrates. The lowest astrocyte presence was observed on P-IBU(3) formulations after 3 days in culture (4.8 ± 0.6%), significantly lower than on bare Pt substrates (55.0 ± 2.9%) and all other PEDOP formulations. Since the high percentage of a specific type of cells at an early time point should be associated with enhanced adhesion of cells to the surface, it could be stated that the surfaces

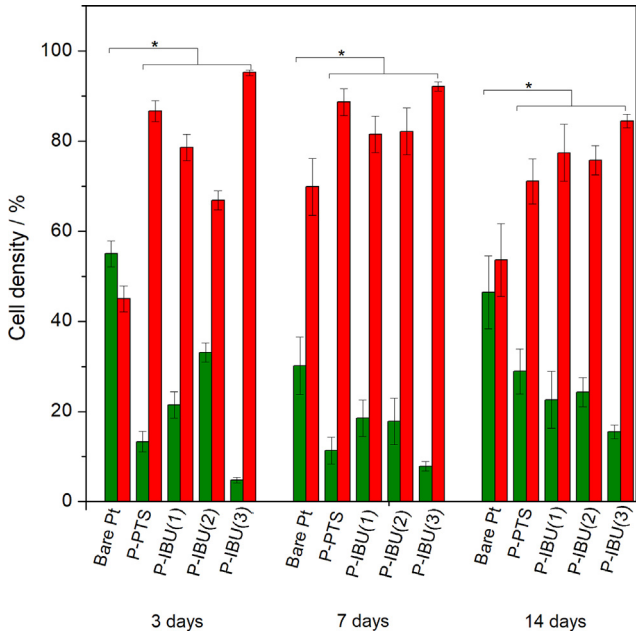

Fig. 6. Cell density analysis of astrocyte (green) and neuron (red) presence on Pt, P-PTS, P-IBU(1), P-IBU(2) and P-IBU(3) after 3, 7 and 14 days of culture; results are presented as the mean ± STD, ★ = $p < 0.05$, n = 3.

of P-IBU(3), P-PTS and P-IBU(1) exhibit specific interactions with neurons. Interestingly, the surface of P-IBU(2) seems to increase the adhesion of neurons less efficiently than other PEDOP formulations, and this could be associated with its surface morphology, which was shown to be the most compact among all investigated PEDOP formulations. On the surface of a bare Pt electrode, the ratio between neurons and astrocytes is close to 1:1, showing no specific interactions of this substrate with a particular type of cells.

The next two time points (7 and 14 days) represent the growth and the development of cell population, in which the density of neurons and astrocytes should be balanced to form a healthy neural environment. The surface of a bare Pt electrode was shown to initially favour the development of neurons, but after 14 days the ratio between astrocytes and neurons was again equal to approx. 1:1. Apart from P-IBU(1), for which there was no significant change in cell density in time, other PEDOP formulations showed the increase in the average percentage of astrocytes. Although astrocyte presence was observed to increases with time, reaching 15.5 ± 1.5% after 14 days in culture, it remained significantly lower on P-IBU(3) relative to Pt substrates, indicating that these PEDOP materials may promote the development of a healthy neural environment. The similar cell density of astrocyte and neuron populations was observed on the surface of PEDOT doped with dexamethasone and decorated with Au particles [49]. Although dexamethasone is a potent anti-inflammatory corticosteroid commonly used in the field of neural devices, when administrated systemically it is found to cause serious side effects, including myopathy and diabetes [50]. Ibuprofen, as a non-steroidal anti-

inflammatory over-the-counter drug, possessing similar ability to reduce tissue reactions following electrode implantation, can be considered as a safe alternative to dexamethasone. Immunofluorescent analysis (Fig. 7A–E) was subsequently performed to quantify the mean neuron number (Fig. 7F) and the mean area of the astrocyte cell body (Fig. 7G) in mixed neural populations cultured on all experimental and control PEDOP formulations. Here, the number of neurons was observed to be the highest on P-IBU(3) formulations relative to other experimental PEDOP formulations and a control material, indicating that P-IBU(3) formulations promoted neural adhesion in vitro. Indeed, after 14 days in culture a ~ 6x increase in neuron presence was observed on the surface of P-IBU(3) formulations relative to bare Pt electrodes, and a ~ 2x increase in neuron presence relative to other experimental PEDOP formulations. Therefore, P-IBU(3) was found to outperform other electrode materials intended for neural applications, e.g. polyhy-

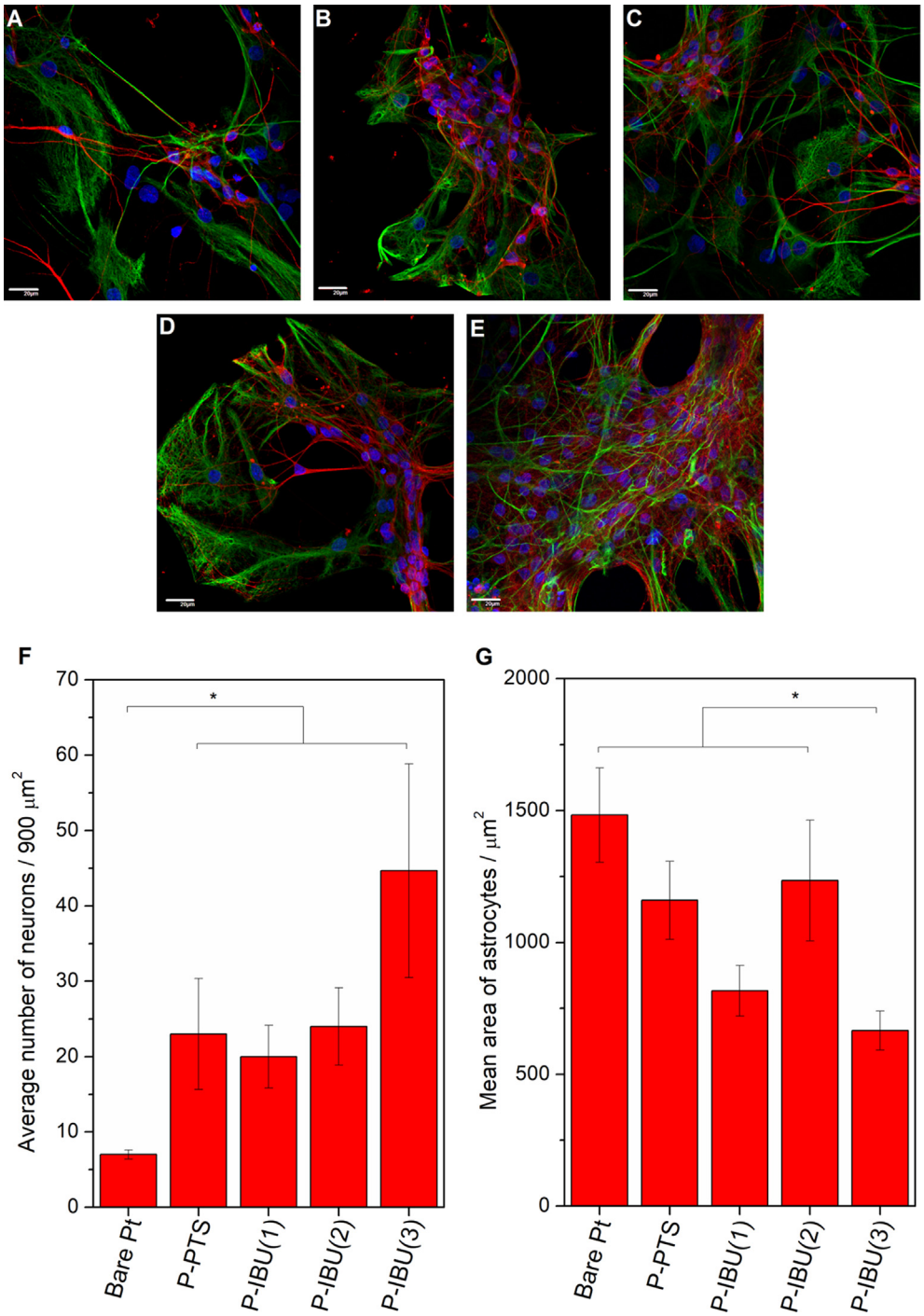

Fig. 7. Representative fluorescent images of primary ventral mesencephalic (VM) mixed cell population cultured for 14 days on Pt (A), P-PTS (B), P-IBU(1) (C), P-IBU(2) (D) and P-IBU(3) (E); neurons are visualized by anti β-tubulin III (red), astrocyte cells by anti-glial fibrillar acidic protein, GFAP stain (green) and nuclei by 4′,6-diamidino-2-phenylindole, DAPI (blue); the scale bar is 20 μm. The average number of neurons over the area of 900 μm^2 (F) and the mean area of astrocytes in μm^2 (G) after 14 days in culture on Pt, P-PTS, P-IBU(1), P-IBU(2) and P-IBU(3); results are presented as the mean ± SEM, ★ = $p < 0.05$, n = 20.

droxyalkanoate/carbon nanotube nanocomposites, for which a ~ 3x increase in neuron presence was observed relative to bare Pt electrodes [29].

An increase in the size of the astrocyte soma is associated with astrocyte activation [48] and can be employed to assess neuroinflammation in vitro. Here, the analysis of the mean astrocyte cell area was performed to assess the anti-inflammatory function of IBU doped PEDOP films (Fig. 7G). It was observed that astrocytes cultured on P-IBU(3) formulations possessed a mean cell area of 666 ± 74 μm^2, significantly less that than astrocytes cultured on bare Pt electrodes (1483 ± 179 μm^2), and similarly to astrocytes cultured on self-supporting CNT films (637 ± 54 μm^2) introduced previously by our group as a material able to prevent reactive gliosis due to its mechanical biomimicry [51]. Also P-IBU(1) formulations were observed to reduce the mean astrocyte cell area (819 ± 95 μm^2), indicating that this PEDOP formulation also possesed an anti-inflammatory functionality. Interestingly, even though the mean area of astrocytes cultured on P-PTS and P-IBU (2) was moderately reduced relative to neural populations cultured on bare Pt substrates, these changes were not statisticaly significant.

4. Conclusions

In this study, the electrochemical and biological effects of ibuprofen doping on poly(3,4-ethylenedioxypyrrole) thin film substrates was assessed in vitro. It was observed that PEDOP formulations formed via a three-step IBU doping/immobilization protocol, P-IBU(3), exhibited the highest CSC (30 ± 1 mC/cm^2) relative to all other experimental PEDOP formulations and control substrates. Although all PEDOP formulations were shown to possess a significantly decreased electrochemical impedance modulus relative to Pt substrates, P-IBU(3) formulations exhibited a significant increase in a double layer capacitance (645.0 ± 51.1 μF) which was associated with its developed surface topography. Characterisation of the total drug loading capacity indicated that different PEDOP formulations were able to immobilize from 150 μg/ml (P-IBU(3)) to 250 μg/ml (P-IBU(2)) of IBU, and elute 95% of loaded drug within circa 20 days. With the release rate constant of 0.15 1/h, P-IBU(3) was found to provide the optimal amount of drug necessary to promote the development of a healthy neural environment and to prevent the activation of astrocytes. Consequently, P-IBU(3) formulations formed via a three-step drug immobilization protocol could be considered as the most beneficial and the safest drug eluting system among all investigated IBU-loaded PEDOP matrices for applications in neural drug delivery.

Declaration of Competing Interest

The authors declare that they have no known competing financial interests or personal relationships that could have appeared to influence the work reported in this paper.

Acknowledgements

This publication has emanated from research conducted with the financial support of Science Foundation Ireland and is cofunded under the European Regional Development Fund under Grant Number 13/RC/2073. This project has received funding from the European Union's Horizon 2020 research and innovation programme under the Marie Skłodowska-Curie grant agreement No 713690 and SFI Technology Innovation Development Programme, grant no.15/TIDA/2992. This work has been supported by the Polish National Science Centre in the framework of Sonata 2016/23/D/ST5/01306. The authors acknowledge the facilities and scientific and technical assistance of the Centre for Microscopy & Imaging at the National University of Ireland Galway, a facility that is funded by NUIG and the Irish Government's Programme for Research in Third Level Institutions, Cycles 4 and 5, National Development Plan 2007-2013.

Appendix A. Supplementary material

Supplementary data to this article can be found online at https://doi.org/10.1016/j.bioelechem.2020.107528.

References

[1] B.S. Mietto, K. Mostacada, A.M.B. Martinez, Neurotrauma and inflammation: CNS and PNS responses, Mediators Inflamm. 2015 (2015), https://doi.org/10.1155/2015/251204 251204.
[2] S.D. Skaper, L. Facci, M. Zusso, P. Giusti, An inflammation-centric view of neurological disease: beyond the neuron, Front. Cell. Neurosci. 12 (2018) 72, https://doi.org/10.3389/fncel.2018.00072.
[3] F.L. Maclean, M.K. Horne, R.J. Williams, D.R. Nisbet, Review: Biomaterial systems to resolve brain inflammation after traumatic injury, APL Bioeng. 2 (2018), https://doi.org/10.1063/1.5023709 021502.
[4] A. Rana, A.E. Musto, The role of inflammation in the development of epilepsy, J. Neuroinflamm. 15 (2018) 144, https://doi.org/10.1186/s12974-018-1192-7.
[5] G.G. Ortiz, H. González-Usigli, F.P. Pacheco-Moisés, M.A. Mireles-Ramírez, A.L. Sánchez-López, E.D. Torres-Sánchez, E.D. González-Renovato, L.J. Flores-Alvarado, M.Á. Macías-Islas, P. Rivero-Moragrega, V.S. González, Physiology and pathology of neuroimmunology: role of inflammation in Parkinson's Disease, Physiol. Pathol. Immunol. (2017), https://doi.org/10.5772/intechopen.70377.
[6] O. Aktas, O. Ullrich, C. Infante-Duarte, R. Nitsch, F. Zipp, Neuronal damage in brain inflammation, Arch. Neurol. 64 (2007) 185–189, https://doi.org/10.1001/archneur.64.2.185.
[7] T.B. Bassani, M.A.B.F. Vital, L.K. Rauh, Neuroinflammation in the pathophysiology of Parkinson's disease and therapeutic evidence of anti-inflammatory drugs, Arq. Neuropsiquiatr. 73 (2015) 616–623, https://doi.org/10.1590/0004-282x20150057.
[8] M.A. Ajmone-Cat, A. Bernardo, A. Greco, L. Minghetti, Non-steroidal anti-inflammatory drugs and brain inflammation: Effects on microglial functions, Pharmaceuticals. 3 (2010) 1949–1964, https://doi.org/10.3390/ph3061949.
[9] D. Dokmeci, Ibuprofen and Alzheimer's disease, Folia Med. (Plovdiv) 46 (2004) 5–10.
[10] H. Bessler, D. Cohen-Terica, M. Djaldetti, P. Sirota, The effect of ibuprofen on cytokine production by mononuclear cells from schizophrenic patients, Folia Biol. (Czech Republic) 63 (2017) 13–19.
[11] U. Wallenquist, K. Holmqvist, A. Hnell, N. Marklund, L. Hillered, K. Forsberg-Nilsson, Ibuprofen attenuates the inflammatory response and allows formation of migratory neuroblasts from grafted stem cells after traumatic brain injury, Restor. Neurol. Neurosci. 30 (2012) 9–19, https://doi.org/10.3233/RNN-2011-0606.
[12] E. Ramazani, Z. Tayarani-Najaran, M. Fereidoni, Celecoxib, indomethacin, and ibuprofen prevent 6-hydroxydopamine-induced PC12 cell death through the inhibition of NFκB and SAPK/JNK pathways, Iran J. Basic Med. Sci. 22 (2019) 477–484, https://doi.org/10.22038/IJBMS.2019.34011.8091.
[13] L.S. Mendonça, C. Nóbrega, S. Tavino, M. Brinkhaus, C. Matos, S. Tomé, R. Moreira, D. Henriques, B.K. Kaspar, L.P. de Almeida, Ibuprofen enhances synaptic function and neural progenitors proliferation markers and improves neuropathology and motor coordination in Machado-Joseph disease models, Hum. Mol. Genet. (2019), https://doi.org/10.1093/hmg/ddz097.
[14] R.M. Haley, H.A. von Recum, Localized and targeted delivery of NSAIDs for treatment of inflammation: A review, Exp. Biol. Med. 244 (2019) 433–444, https://doi.org/10.1177/1535370218787770.
[15] A. Puiggalí-Jou, L.J. del Valle, C. Alemán, Drug delivery systems based on intrinsically conducting polymers, J. Control. Release. 309 (2019) 244–264, https://doi.org/10.1016/j.jconrel.2019.07.035.
[16] K. Krukiewicz, A. Kruk, R. Turczyn, Evaluation of drug loading capacity and release characteristics of PEDOT/naproxen system: Effect of doping ions, Electrochim. Acta. 289 (2018) 218–227.
[17] C. Kleber, K. Lienkamp, J. Rühe, M. Asplund, Electrochemically Controlled Drug Release from a Conducting Polymer Hydrogel (PDMAAp/PEDOT) for Local Therapy and Bioelectronics, Adv. Healthc. Mater. 8 (2019), https://doi.org/10.1002/adhm.201801488 e1801488.
[18] K. Krukiewicz, P. Zawisza, A.P. Herman, R. Turczyn, S. Boncel, J.K. Zak, An electrically controlled drug delivery system based on conducting poly(3,4-ethylenedioxypyrrole) matrix, Bioelectrochemistry. 108 (2016) 13–20, https://doi.org/10.1016/j.bioelechem.2015.11.002.
[19] K. Krukiewicz, J.K. Zak, Conjugated polymers as robust carriers for controlled delivery of anti-inflammatory drugs, J. Mater. Sci. 49 (2014) 5738–5745, https://doi.org/10.1007/s10853-014-8292-2.
[20] K. Krukiewicz, B. Gniazdowska, T. Jarosz, A.P. Herman, S. Boncel, R. Turczyn, Effect of immobilization and release of ciprofloxacin and quercetin on

electrochemical properties of poly(3,4-ethylenedioxypyrrole) matrix, Synth. Met. 249 (2019) 52–62, https://doi.org/10.1016/j.synthmet.2019.02.001.
[21] N. Rozlosnik, New directions in medical biosensors employing poly(3,4-ethylenedioxy thiophene) derivative-based electrodes, Anal. Bioanal. Chem. 395 (2009) 637–645, https://doi.org/10.1007/s00216-009-2981-8.
[22] K. Krukiewicz, A. Kowalik, D. Czerwińska-Główka, M.J.P. Biggs, Electrodeposited poly(3,4-ethylenedioxypyrrole) films as neural interfaces: Cytocompatibility and electrochemical studies, Electrochim. Acta. 302 (2019) 21–30, https://doi.org/10.1016/j.electacta.2019.02.023.
[23] K. Krukiewicz, A. Stokfisz, J.K. Zak, Two approaches to the model drug immobilization into conjugated polymer matrix, Mater. Sci. Eng. C. Mater. Biol. Appl. 54 (2015) 176–181, https://doi.org/10.1016/j.msec.2015.05.017.
[24] A.S. Bondarenko, G.A. Ragoisha, EIS Spectrum Analyser, Prog. Chemom. Res. (2005) 89–102.
[25] K. Krukiewicz, M. Chudy, G. Stephen, M.J.P. Biggs, The Synergistic Effects of Gold Particles and Dexamethasone on the Electrochemical and Biological Performance of PEDOT Neural Interfaces, Polymers (Basel). 11 (2019) 67.
[26] R.W. Korsmeyer, R. Gurny, E. Doelker, P. Buri, N.A. Peppas, Mechanisms of solute release from porous hydrophilic polymers, Int. J. Pharm. 15 (1983) 25–35, https://doi.org/10.1016/0378-5173(83)90064-9.
[27] E. Shamaeli, N. Alizadeh, Kinetic studies of electrochemically controlled release of salicylate from nanostructure conducting molecularly imprinted polymer, Electrochim. Acta. 114 (2013) 409–415, https://doi.org/10.1016/j.electacta.2013.10.119.
[28] C. Vallejo-Giraldo, N.P. Pampaloni, A.R. Pallipurath, P. Mokarian-Tabari, J. O'Connell, J.D. Holmes, A. Trotier, K. Krukiewicz, G. Orpella-Aceret, E. Pugliese, L. Ballerini, M. Kilcoyne, E. Dowd, L.R. Quinlan, A. Pandit, P. Kavanagh, M.J.P. Biggs, Preparation of Cytocompatible ITO Neuroelectrodes with Enhanced Electrochemical Characteristics Using a Facile Anodic Oxidation Process, Adv. Funct. Mater. 28 (2017) 1605035, https://doi.org/10.1002/adfm.201605035.
[29] C. Vallejo-Giraldo, E. Pugliese, A. Larrañaga, M.A. Fernandez-Yague, J.J. Britton, A. Trotier, G. Tadayyon, A. Kelly, I. Rago, J.R. Sarasua, E. Dowd, L.R. Quinlan, A. Pandit, M.J.P. Biggs, Polyhydroxyalkanoate/carbon nanotube nanocomposites: flexible electrically conducting elastomers for neural applications, Nanomedicine 11 (2016) 2547–2563, https://doi.org/10.2217/nnm-2016-0075.
[30] J. Arle, J. Shils, Essential Neuromodulation, 2011. doi:10.1016/C2009-0-61346-5.
[31] B.N. Reddy, M. Deepa, Unraveling nanoscale conduction and work function in a poly(3,4- ethylenedioxypyrrole)/carbon nanotube composite by Kelvin probe force microscopy and conducting atomic force microscopy, Electrochim. Acta. 70 (2012) 228–240, https://doi.org/10.1016/j.electacta.2012.03.051.
[32] A. Kumar, R.K. Singh, H.K. Singh, P. Srivastava, R. Singh, Enhanced capacitance and stability of p-toluenesulfonate doped polypyrrole/carbon composite for electrode application in electrochemical capacitors, J. Power Sour. 246 (2014) 800–807, https://doi.org/10.1016/j.jpowsour.2013.07.121.
[33] J.M. Alía, H.G.M. Edwards, B.M. Kiernan, Raman spectroscopy of benzenesulfonic and 4-toluenesulfonic acids dissolved in dimethylsulfoxide, Spectrochim. Acta - Part A Mol. Biomol Spectrosc. 60 (2004) 1533–1542, https://doi.org/10.1016/j.saa.2003.08.016.
[34] A. Jubert, M.L. Legarto, N.E. Massa, L.L. Tévez, N.B. Okulik, Vibrational and theoretical studies of non-steroidal anti-inflammatory drugs Ibuprofen [2-(4-isobutylphenyl)propionic acid]; Naproxen [6-methoxy-α-methyl-2-naphthalene acetic acid] and Tolmetin acids [1-methyl-5-(4-methylbenzoyl)-1H-pyrrole-2-acetic acid], J. Mol. Struct. 783 (2006) 34–51, https://doi.org/10.1016/j.molstruc.2005.08.018.
[35] Y. Xiao, X. Cui, J.M. Hancock, M. Bouguettaya, J.R. Reynolds, D.C. Martin, Electrochemical polymerization of poly(hydroxymethylated-3,4-ethylenedioxythiophene) (PEDOT-MeOH) on multichannel neural probes, Sens. Actuat. B Chem. 99 (2004) 437–443, https://doi.org/10.1016/j.snb.2003.12.067.
[36] T. Schoetz, M. Kurniawan, M. Stich, R. Peipmann, I. Efimov, A. Ispas, A. Bund, C. Ponce De Leon, M. Ueda, Understanding the charge storage mechanism of conductive polymers as hybrid battery-capacitor materials in ionic liquids by: In situ atomic force microscopy and electrochemical quartz crystal microbalance studies, J. Mater. Chem. A. 6 (2018) 17787–17799, https://doi.org/10.1039/c8ta06757k.
[37] M.L. Bruschi, Mathematical models of drug release, in: Strateg. to Modify Drug Release from Pharm. Syst., Woodhead Publishing, 2015, pp. 63–86, 10.1016/b978-0-08-100092-2.00005-9.
[38] Y. Fu, W.J. Kao, Drug release kinetics and transport mechanisms of non-degradable and degradable polymeric delivery systems, Expert Opin. Drug Deliv. 7 (2010) 429–444, https://doi.org/10.1517/17425241003602259.
[39] B. Adnadjevic, J. Jovanovic, A comparative kinetics study of isothermal drug release from poly(acrylic acid) and poly(acrylic-co-methacrylic acid) hydrogels, Colloids Surf. B Biointerf. 69 (2009) 31–42, https://doi.org/10.1016/j.colsurfb.2008.10.018.
[40] X. Gao, L. Lei, D. O'Hare, J. Xie, P. Gao, T. Chang, Intercalation and controlled release properties of vitamin C intercalated layered double hydroxide, J. Solid State Chem. 203 (2013) 174–180, https://doi.org/10.1016/j.jssc.2013.04.028.
[41] G. Cirillo, M. Curcio, U.G. Spizzirri, O. Vittorio, P. Tucci, N. Picci, F. Iemma, S. Hampel, F.P. Nicoletta, Carbon nanotubes hybrid hydrogels for electrically tunable release of Curcumin, Eur. Polym. J. 90 (2017) 1–12, https://doi.org/10.1016/j.eurpolymj.2017.03.011.
[42] N. Alizadeh, E. Shamaeli, Electrochemically controlled release of anticancer drug methotrexate using nanostructured polypyrrole modified with cetylpyridinium: Release kinetics investigation, Electrochim. Acta 130 (2014) 488–496, https://doi.org/10.1016/j.electacta.2014.03.055.
[43] B. Alshammary, N. Casillas, R.B. Cook, J. Swingler, C. Ponce de León, F.C. Walsh, The importance of the film structure during self-powered ibuprofen salicylate drug release from polypyrrole electrodeposited on AZ31 Mg, J. Solid State Electrochem. 20 (2016) 3375–3382, https://doi.org/10.1007/s10008-016-3288-2.
[44] E. Shamaeli, N. Alizadeh, Functionalized gold nanoparticle-polypyrrole nanobiocomposite with high effective surface area for electrochemical/pH dual stimuli-responsive smart release of insulin, Colloids Surf. B Biointerf. 126 (2015) 502–509, https://doi.org/10.1016/j.colsurfb.2015.01.003.
[45] E. Shamaeli, N. Alizadeh, Nanostructured biocompatible thermal/electrical stimuli-responsive biopolymer-doped polypyrrole for controlled release of chlorpromazine: kinetics studies, Int. J. Pharm. 472 (2014) 327–338, https://doi.org/10.1016/j.ijpharm.2014.06.036.
[46] V. Papadopoulou, K. Kosmidis, M. Vlachou, P. Macheras, On the use of the Weibull function for the discernment of drug release mechanisms, Int. J. Pharm. 309 (2006) 44–50, https://doi.org/10.1016/j.ijpharm.2005.10.044.
[47] M. Berns, M. Toennessen, P. Koehne, R. Altmann, M. Obladen, Ibuprofen augments bilirubin toxicity in rat cortical neuronal culture, Pediatr. Res. 65 (2009) 392–396, https://doi.org/10.1203/PDR.0b013e3181991511.
[48] D.J. DiSabato, N. Quan, J.P. Godbout, Neuroinflammation: the devil is in the details, J. Neurochem. 139 (2016) 136–153, https://doi.org/10.1111/jnc.13607.
[49] K. Krukiewicz, M. Chudy, C. Vallejo-Giraldo, M. Skorupa, D. Więcławska, R. Turczyn, M. Biggs, Fractal form PEDOT/Au assemblies as thin-film neural interface materials, Biomed. Mater. 13 (2018) 54102. http://stacks.iop.org/1748-605X/13/i=5/a=054102.
[50] P.J. Koehler, Use of corticosteroids in neuro-oncology, Anticancer. Drugs. 6 (1995) 19–33, https://doi.org/10.1097/00001813-199502000-00002.
[51] K. Krukiewicz, D. Janas, C. Vallejo-Giraldo, M.J.P. Biggs, Self-supporting carbon nanotube films as flexible neural interfaces, Electrochim. Acta. 295 (2019) 253–261, https://doi.org/10.1016/j.electacta.2018.10.157.